DOI: 10.1002/ejic.200700924

Metal Coordination Architectures of 2,3-Bis(triazol-1-ylmethyl)quinoxaline: Effect of Metal Ion and Counterion on Complex Structures

Jian-Long Du,[a] Tong-Liang Hu,[a] Jian-Rong Li,[a] Shu-Ming Zhang,[a] and Xian-He Bu*[a]

Keywords: Counterions / Crystal structure / Flexible ligands / Synthesis / Weak interactions / Ligand design

A series of complexes, $[Zn\mathbf{L}Cl_2]_2$ (**1**), $[Zn\mathbf{L}_2(NO_3)_2]_\infty$ (**2**), $[Mn\mathbf{L}_2(NO_3)_2]_\infty$ (**3**), $\{[Zn\mathbf{L}_2(H_2O)_2](ClO_4)_2(CH_3COCH_3)_2\}_\infty$ (**4**), $\{[Mn\mathbf{L}_2(H_2O)_2](ClO_4)_2(CH_3COCH_3)_2\}_\infty$ (**5**), $\{[Cd\mathbf{L}_2(H_2O)_2](ClO_4)_2(H_2O)_6\}_\infty$ (**6**), and $\{[Ag\mathbf{L}](ClO_4)(H_2O)_{1.5}\}_\infty$ (**7**), based on the flexible ligand 2,3-bis(triazol-1-ylmethyl)quinoxaline (**L**) were synthesized and characterized by elemental analyses, IR spectroscopy, thermogravimetric analyses, and single-crystal X-ray diffraction. Complex **1** is a dinuclear macrocyclic molecular, which is further linked into a 1D supramolecular chain by intermolecular C–H···Cl weak interactions. The metal centers in **2** and **3** coordinate two NO_3^- anions, and the flexible ligand bridges $M(NO_3)_2$ [M = Zn^{II} or Mn^{II}] units to form 1D chain structures. Complexes **4**, **5**, and **6** show a 2D network structure with (4,4) topology. As expected, complex **7** has a 1D strand chain structure that is different than other M^{II} complexes (**4**, **5**, and **6**) with the same ligand. These chains are further extended into a 2D supramolecular network by O···Ag···O weak interactions. In all these complexes, the ligand bridges in a similar mode; however, the complexes have different structures ranging from a dinuclear structure to a 2D network mainly due to the differences in the coordination geometries of the metal centers and counterions. These results reveal that the coordination geometry of metal ions and the coordinating abilities of the counterions play important roles in defining the overall structure of metal–organic frameworks. In addition, the fluorescent properties of complexes **1**, **2**, **4**, **6**, **7**, and ligand **L** and the EPR spectra of complex **5** were also investigated.

Introduction

In the past decades, metal–organic frameworks (MOFs) have attracted considerable interest not only for their diversity of architectures and topologies, but also for their fascinating potential application as functional materials.[1,2] The structures of such complexes mainly depend on the characteristics of their building blocks.[3] Many factors such as metal ions,[4] the structure of the organic ligands,[5] counteranions,[6] solvents,[7] metal/ligand ratio,[8] pH value,[9] and even reaction temperatures[10] have been found to remarkably influence the structural topologies of the resultant coordination frameworks. In particular, the role of the anions in self-assembly processes has emerged as an increasingly active theme in recent studies.[11] Accordingly, the understanding of the intriguing connection between complex structures and the factors affecting the formation of the framework is one of the key points for the rational design of crystalline materials, but this still seems to be a long-term challenge.

Recently, many studies have been carried out with the use of flexible bridging ligands to build coordination architectures.[12] Flexible spacers allow ligands to bend or rotate when coordinating to metal centers to conform to the coordination geometries of the metal ions. The reactions of such ligands (especially those containing S, N, or O donors) with appropriate metal ions under the proper synthetic conditions have led to many kinds of structures, such as discrete cycles, chains, or helices.[12,13] The bis(imidazol) and bis(triazol) ligands bearing flexible spacers are good N-donor ligands, and significant progress has been achieved by Robson and others.[14] An infinite 2D polyrotaxane network of $Ag_2(bix)_3(NO_3)_2$ [bix = 1,4-bis(imidazol-1-ylmethyl)benzene] and a series of Cd–btx complexes [btx = 1,4-bis(trizol-1-ylmethyl)benzene] with third-order NLO (nonlinear optics) properties and fluorescence properties have been reported.[15]

In our previous work, some ligands with flexible spacers were successfully used to construct various structures of complexes including discrete molecules, 1D, 2D, and 3D networks, and some of the coordination polymers showed interesting fluorescence properties.[16] We reported complexes bearing a 9,10-bis(triazol-1-ylmethyl)anthracene unit and examined their fluorescence properties.[16a] In order to systematically study the influence of metal ions, ligand spacers, and counteranions on the structure and properties of metal–organic complexes, in this paper, the flexible 2,3-bis(triazol-1-ylmethyl)quinoxaline (**L**) ligand (Figure 1) was designed, and seven metal complexes with the ligand,

[a] Department of Chemistry, Nankai University, Tianjin 300071, P. R. China
Fax: +86-22-23502458
E-mail: buxh@nankai.edu.cn
Supporting information for this article is available on the WWW under http://www.eurjic.org or from the author.

$[ZnLCl_2]_2$ (**1**), $[ML_2(NO_3)_2]_\infty$ [M = Zn^{II} (**2**), Mn^{II} (**3**)], $\{[ML_2(H_2O)_2](ClO_4)_2(CH_3COCH_3)_2\}_\infty$ [M = Zn^{II} (**4**), Mn^{II} (**5**)], $\{[CdL_2(H_2O)_2](ClO_4)_2(H_2O)_6\}_\infty$ (**6**), and $\{[AgL](ClO_4)(H_2O)_{1.5}\}_\infty$ (**7**) were synthesized and structurally characterized. Furthermore, the fluorescence properties of complexes **1**, **2**, **4**, **6**, and **7** and the EPR spectra of complex **5** were investigated in the solid state at room temperature.

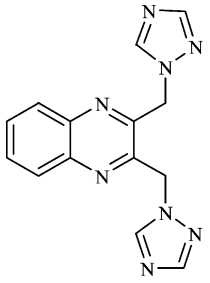

Figure 1. The flexible 2,3-bis(triazol-1-ylmethyl)quinoxaline ligand.

Results and Discussion

Syntheses Consideration and General Characterizations

Recently, we investigated the ligand 9,10-bis(triazol-1-ylmethyl)anthracene, and the emission properties of complexes based on this ligand were reported.[16a] Simultaneously, some complexes with the related 1,4-bis(triazol-1-ylmethyl)benzene ligand and their third-order nonlinear optical properties were reported.[15a] In order to explore the influence of ligand nature on crystal structures of their metal complexes, the new flexible ligand 2,3-bis(triazol-1-ylmethyl)quinoxaline (**L**) was designed and synthesized.

Ligand **L** can be conveniently prepared by a substitution reaction between 1*H*-1,2,4-triazole and 2,3-bis(bromomethyl)quinoxaline under strong alkaline (KOH) conditions. Excessive triazole was used to reduce the monosubstituted product. The chemical composition and purity of the ligand were confirmed by NMR and IR spectroscopy and elemental analyses.

Treatment of ligand **L** with Zn^{II}, Cd^{II}, Mn^{II}, and Ag^{I} salts afforded complexes **1**–**7**, which were characterized by elemental analyses, IR spectroscopy, and X-ray single-crystal diffraction analyses. All complexes are air stable at room temperature. Although all the reactions of metal salts with the **L** ligand were carried out under similar conditions in a molar ratio of 1:1, the isolated compounds had different stoichiometry.

The infrared spectra of **1**–**7** all exhibit the characteristic absorptions for **L** with a slight shift due to the coordination. In **2** and **3**, the absorption band appeared at 1370 cm^{-1}, and a value of 1375 cm^{-1} is characteristic of the coordinated NO_3^- anions. The absorption bands at ca. 624 and ca. 1100 cm^{-1} indicate the existence of the ClO_4^- anion in **4**, **5**, **6**, and **7**.

Descriptions of Crystal Structures

[ZnLCl$_2$]$_2$ (1)

Complex **1** crystallizes in the triclinic symmetry with $P\bar{1}$ space group. Selected bond lengths and angles are shown in Table 1. X-ray single-crystal diffraction analysis revealed that **1** has a dinuclear structure constructed from two $ZnCl_2$ units and two **L** ligands. As shown in Figure 2a, the Zn^{II} ions are located in a distorted tetrahedral geometry, and

Table 1. Selected bond lengths [Å] and angles [°] for complexes **1**–**7**.[a]

1			
Zn1–N2	2.0246(19)	Zn1–N7#1	2.0265(19)
Zn1–Cl2	2.2266(8)	Zn1–Cl1	2.2334(8)
N2–Zn1–N7#1	101.76(7)	N2–Zn1–Cl2	107.16(6)
N7#1–Zn1–Cl2	110.02(6)	N2–Zn1–Cl1	109.89(6)
N7#1–Zn1–Cl1	106.66(6)	Cl2–Zn1–Cl1	119.88(3)
2			
Zn1–N1	2.137(2)	Zn1–N7#1	2.125(2)
Zn1–O1	2.1656(19)		
N7#1–Zn1–N1	92.73(8)	N7#2–Zn1–N1	87.27(8)
N1–Zn1–O1#3	93.80(8)	N7#1–Zn1–O1	87.27(8)
N7#2–Zn1–O1	92.73(8)	N1–Zn1–O1	86.20(8)
3			
Mn1–N1	2.133(3)	Mn1–N8#2	2.146(3)
Mn1–O1	2.170(3)		
N1–Mn1–N8#3	92.73(14)	N1–Mn1–N8#2	87.27(14)
N8#2–Mn1–O1	93.80(13)	N1–Mn1–O1	87.42(14)
N1–Mn1–O1#1	92.58(14)	N8#3–Mn1–O1	86.20(13)
4			
Zn1–N1	2.185(3)	Zn1–O1W	2.183(3)
Zn1–N8#1	2.107(3)		
N8#1–Zn1–O1W	92.00(13)	N8#2–Zn1–O1W	88.00(13)
N8#1–Zn1–N1	88.10(12)	N8#2–Zn1–N1	91.90(12)
O1W#3–Zn1–N1	91.20(13)	O1W–Zn1–N1	88.80(13)
5			
Mn1–N1	2.275(4)	Mn1–N8#1	2.233(3)
Mn1–O1W	2.235(3)		
N8#2–Mn1–O1W	91.90(13)	N8#1–Mn1–O1W	88.10(13)
N8#2–Mn1–N1	87.62(13)	N8#1–Mn1–N1	92.38(13)
O1W–Mn1–N1	88.24(13)	O1W#3–Mn1–N1	91.76(13)
6			
Cd1–N1	2.317(4)	Cd1–N7#2	2.272(5)
Cd1–O1W	2.334(4)		
N7#2–Cd1–O1W	91.69(17)	N7#3–Cd1–O1W	88.31(17)
N7#2–Cd1–N1	87.51(15)	N7#3–Cd1–N1	92.49(15)
N1–Cd1–O1W	87.56(16)	N1#4–Cd1–O1W	92.44(16)
7			
Ag1–N2	2.141(10)	N2–Ag1–N8#2	167.8(4)
Ag1–N8#2	2.135(11)	C2–N2–Ag1	125.4(9)

[a] Symmetry code for **1**: #1 $-x, -y+1, -z+1$. **2**: #1 $-x+1/2, y, -z+3/2$; #2 $x-1/2, -y+1, z-1/2$; #3 $-x, -y+1, -z+1$. **3**: #1 $-x+1, -y, -z+1$; #2 $x+1/2, -y, z+1/2$; #3 $-x+1/2, y, -z+1/2$. **4**: #1 $x, -y+2, z-1/2$; #2 $-x+1/2, y-1/2, -z+1/2$; #3 $-x+1/2, -y+3/2, -z$; #4 $-x+1/2, -y+1/2, -z+1/2$. **5**: #1 $-x+1/2, y+1/2, -z+1/2$; #2 $x, -y+1, z+1/2$; #3 $-x+1/2, -y+3/2, -z+1$; #4 $-x+1/2, y-1/2, -z+1/2$. **6**: #1 $-x+1/2, y-1/2, -z+1/2$; #2 $x, -y, z+1/2$; #3 $-x+1/2, y+1/2, -z+1/2$; #4 $-x+1/2, -y+1/2, -z+1$. **7**: #1 $x, y-1, z$; #2 $x, y+1, z$.

they are coordinated to two Cl^- anions and two triazole N donors of two **L** ligands; the Zn–N bond lengths are 2.0246(19) and 2.0265(19) Å (Table 1). The packing diagram reveals a discrete dimeric unit involving intermolecular C–H···Cl contacts (C11–H11B···Cl1 135.2°, C11···Cl1 3.510 Å; C15–H15···Cl1 126.8°, C15···Cl1 3.466 Å), and then individual molecules through C–H···Cl hydrogen bonds to form an infinite 1D chain (Figure 2b).[17]

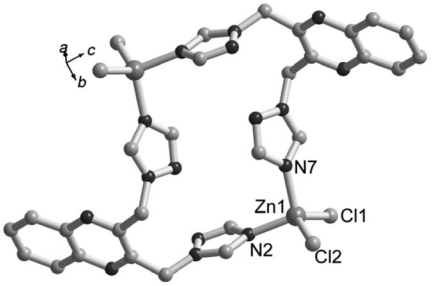

(a)

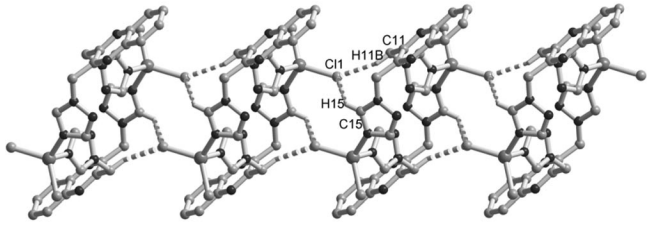

(b)

Figure 2. View of (a) the coordination environment of Zn^{II} ions in **1**; (b) the 1D chain formed by the C–H···Cl weak interactions (H atoms omitted for clarity).

[ZnL$_2$(NO$_3$)$_2$]$_\infty$ (2) and [MnL$_2$(NO$_3$)$_2$]$_\infty$ (3)

When $ZnCl_2$ was replaced by $Zn(NO_3)_2{\cdot}6H_2O$ or $Mn(NO_3)_2{\cdot}6H_2O$, two 1D structural coordination polymers were obtained (Figure 3). Single-crystal X-ray analyses of **2** and **3** indicate that they are isostructural. Therefore, we used M instead of Zn^{II} and Mn^{II} to describe their structures in this text. Different to the tetrahedral four-coordinate Zn^{II} center in **1**, each metal in **2** (or **3**) is six-coordinate to two oxygen atoms of two distinct nitrate anions [Zn–O 2.1659(19) Å, Mn–O 2.170(3) Å] and four N donors of four **L** ligands [Zn–N 2.125(2)–2.137(2) Å], which is longer than that in **1**; the Mn–N distance is 2.133(3)–2.146(3) Å, which is longer than those of **2** (Figure 3a and Table 1). As shown in Figure 3, the metal center lies in a slightly distorted octahedral environment, and the compound adopts a chain motif; the metal centers are linked together through four **L** ligands into an undulating 1D chain. The individual "links" in the chains consist of M_2L_2 units, which can be viewed as macrocyclic molecules enclosed by two metal ions and two **L** ligands. The interchain Zn···Zn and Mn···Mn separations are 8.547 and 8.543 Å, respectively. Two monodentate NO_3^- anions are located above and below the M_2L_2 ring planes.

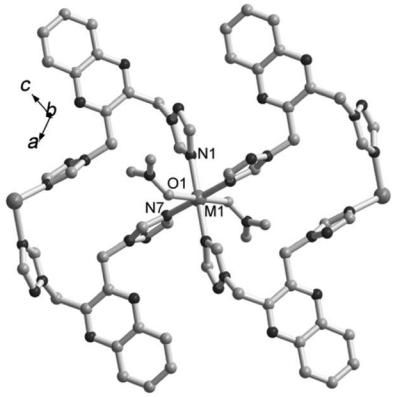

(a)

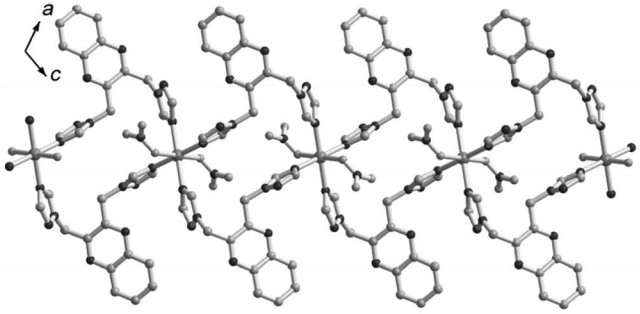

(b)

Figure 3. View of (a) the M^{II} [M = Zn^{II} or Mn^{II}] coordination environment in **2** and **3**; (b) the 1D chain structure of **2** and **3**.

{[ZnL$_2$(H$_2$O)$_2$](ClO$_4$)$_2$(CH$_3$COCH$_3$)$_2$}$_\infty$ (4), {[MnL$_2$(H$_2$O)$_2$](ClO$_4$)$_2$(CH$_3$COCH$_3$)$_2$}$_\infty$ (5), and {[CdL$_2$(H$_2$O)$_2$](ClO$_4$)$_2$(H$_2$O)$_6$}$_\infty$ (6)

The reactions of **L** with $Zn(ClO_4)_2{\cdot}6H_2O$, $Mn(ClO_4)_2{\cdot}6H_2O$, or $Cd(ClO_4)_2{\cdot}6H_2O$ afforded **4**–**6**, respectively. Compounds **4**, **5**, and **6** have similar structures except for different solvent molecules. The packing acetone or water molecules are located at the cavities of the interlayers of **4**, **5**, and **6**, respectively. Herein, we use M instead of Zn^{II}, Mn^{II}, and Cd^{II} to describe their structures later in this text.

Figure 4a shows the coordination environment of the metal ion, which resides at an inversion center and is six-coordinate in a distorted octahedral environment. Two coordinated O atoms from water molecules occupy the axial positions, and the equatorial plane is defined by four N donors from four **L** ligands. Each **L** in turn serves as a bridge to connect two metal ions to form a (4,4) 2D grid layer (Figure 4b). All metal ions in each layer are completely coplanar. The M–M separations are 10.059 (for **4**), 10.188 (for **5**), and 10.180 Å (for **6**) with M2–M1–M4 cor-

ner angles of 49.82, 48.23, and 49.16°, respectively. In each (4,4) grid, four **L** ligands connect four metal ions to form a 44-membered ring. In addition, the uncoordinated ClO_4^- anions are located between two 2D layers to balance the charge. As expected, with a decrease in the radii of the central metal ions, Cd^{II} (1.490 Å), Mn^{II} (1.370 Å), and Zn^{II} (1.330 Å), the axial M–O(water) distances (2.334 Å for **6**, 2.235 Å for **5**, 2.183 Å for **4**) and the equatorial M–N(triazolyl) distances (2.317 and 2.272 Å for **6**, 2.275 and 2.233 Å for **5**, 2.185 and 2.183 Å for **4**) become shorter (Table 1).

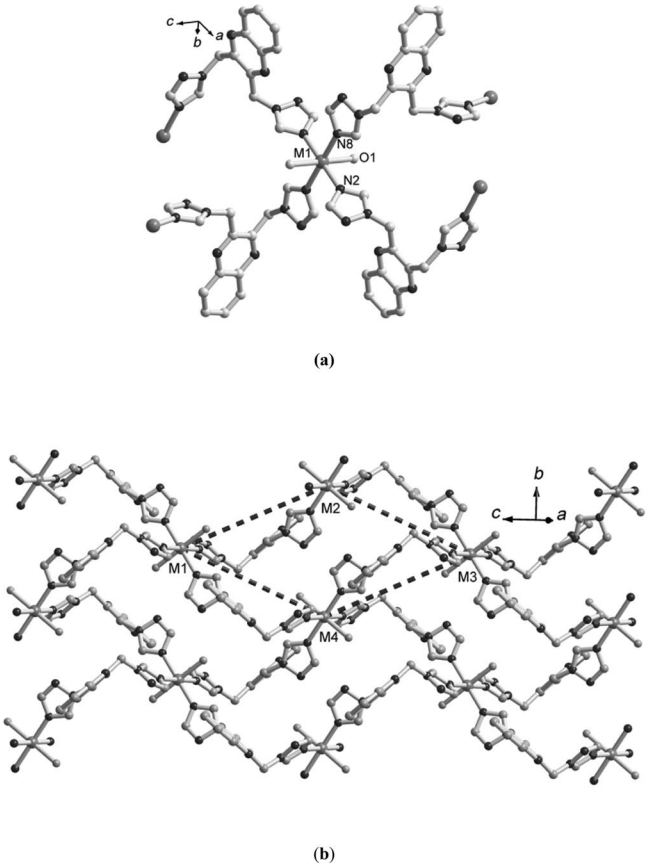

Figure 4. View of (a) the M^{II} [M = Zn^{II}, Mn^{II} or Cd^{II}] coordination environment in **4**, **5**, and **6**; (b) the 2D sheet of **4**, **5**, and **6** (H atoms omitted for clarity).

{[AgL](ClO$_4$)(H$_2$O)$_{1.5}$}$_\infty$ (7)

Complex **7** has a 1D strand-chain structure. Each Ag^I is linked by two N donors from the L ligands [Ag1–N2 2.141(10) Å, Ag1–N8$^{\#2}$ 2.135(11) Å] in a dicoordinated linear fashion as shown in Figure 5a. All ligands are equivalent, and the dihedral angles between the planes of the triazole and quinoxaline units are 77.925 and 76.876°, respectively, whereas the two triazole rings are almost parallel with a dihedral angle of 17.684°. As depicted in Figure 5b, the nearest nonbonding Ag···Ag distance linked by **L** is 13.901 Å, and the N2–Ag1–N8$^{\#2}$ [167.8(4)°] angle confirms the nearly linear coordinated environment of the Ag^I center. It is worth noting that the O atoms of ClO_4^- are not coordinated to the Ag^I ions, but weak interactions are observed between the O atoms and the Ag^I ions; the chains are assembled by O···Ag···O weak interactions between the adjacent chains into an infinite 2D supramolecular sheet (Figure 5b). The Ag···O distances are 2.8250 and 3.1128 Å, and the O···Ag···O angle is 115.477°.

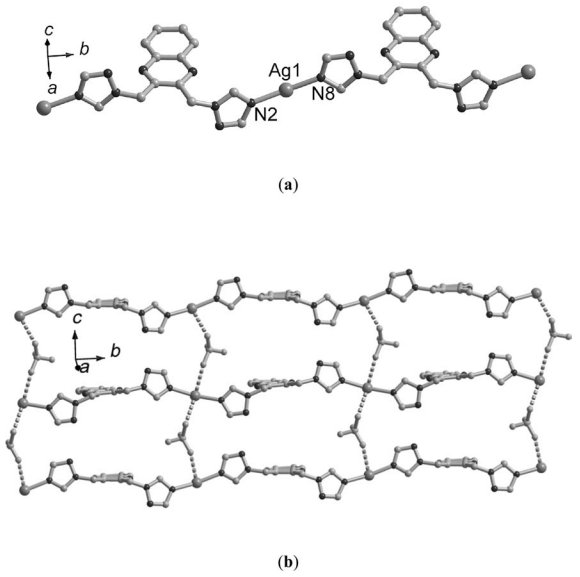

Figure 5. View of (a) the coordination environment of Ag^I in **7**; (b) the 2D sheet of **7** formed by O···Ag···O weak interactions (H atoms omitted for clarity).

The controlled assembly of a metallosupramolecule in crystal engineering has drawn the attention of chemists in recent years, but it is still a great challenge in the field of crystal engineering. As we know, the most common approach to build metal–organic frameworks is the rational combination of organic ligands with appropriate coordination sites and metal ions bearing a specific coordination geometry. It was demonstrated that several other subtle factors also play important roles in the formation of coordination frameworks.

In the present work, the structural differences complexes **1**–**6** show that the central metal ions and counteranions greatly affect the overall structures of the metal–organic frameworks. As can be seen in **1**, the tetrahedral Zn^{II} center coordinates two Cl^- anions and two N donors of the **L** ligand, and complex **1** forms a dinuclear structure with intermolecular weak interactions stabilizing the crystal structure to some extent. A similar dinuclear Zn^{II} complex was also obtained from the self-assembly of the flexible ligand *N*,*N*-bis(3-pyridylmethyl)thiourea with $ZnCl_2$.[6d] The different organic ligands do not seem to have a great effect on the final dinuclear structure in this case. Different than that in **1**, the coordination geometry of the metal center in **2** (and **3**) is octahedral and coordinated by two O donors from NO_3^- and four N donors from the **L** ligand; the complex forms a 1D double-chain coordination network. The Cl^- and NO_3^- anions are coordinated to the metal center as a result of their strong coordination ability relative to that of ClO_4^-, which acts as the counteranion in **4**–**6** because of its poor coordination ability. It should be noted that the coordination geometry of the metal centers in **4**–**6** is very

similar to that of **2** and **3**, but the former forms 2D grid structure, whereas the later forms a 1D chain structure. The template effect of the uncoordinated ClO_4^- ion may be responsible for this result. Moreover, in this reaction system, the different transition-metal ions (Zn^{II}, Cd^{II}, and Mn^{II}) seem to show no significant effect on the complex structures. In contrast, when the spacer of the ligand is changed from quinoxaline to the bulky anthracene [9,10-bis(triazol-1-ylmethyl)anthracene], the $Zn(ClO_4)_2$ complex of this ligand formed a 2D (4,4) grid structure that is similar to that of **4**–**6**.[16a] The Ag^I ion has more types of coordination geometries than many other transition-metal ions, such as linear, trigonal, tetrahedral, pyramidal, octahedral, and so on. For **7**, the linear coordination geometry of the Ag^I ion directs the assembly process, which forms a 1D strand supramolecular structure. Furthermore, the O···Ag···O weak interactions also contribute to form the final crystal structures.

XRPD Results

To confirm the phase purity of the bulk materials, X-ray powder diffraction (XRPD) experiments were carried out for complexes **1**, **2**, **4**–**7**. The experimental and computer-simulated XRPD patterns of the corresponding complexes are shown in Figures S1–S6 in the Supporting Information. Although the experimental patterns have a few unindexed diffraction lines and some are slightly broadened in comparison to those simulated from the single-crystal models, it still can be considered that the bulk of the synthesized materials and the crystals used for diffraction are homogeneous.

Thermogravimetric Analyses

Thermogravimetric analyses (TGA) of **1**, **2**, **4**, **6**, and **7** were performed by heating the corresponding complex under an atmosphere of N_2 with a heating rate of 10 °C min^{-1} between ambient temperature and 800 °C, and the TGA curves are provided as Figures S7–S11 in the Supporting Information. The results show that **1** begin to decompose at 287 °C (for **2** at 189 °C), and the weight loss continues until the temperature is above 600 °C. The TGA curves of **4** and **6** are similar due to their similar structures. There are two separate weight loss steps: the first weight loss of 4.0% occurs from 25 to 200 °C, which may be attributed to the loss of the solvent water molecules, and the second one corresponds to the decomposition of the complexes at higher temperatures (550 °C for **4**, 630 °C for **6**). Complex **7** loses the solvent water molecules below 150 °C with the first weight loss of 1.8% (calcd. 1.64%), and then decomposes above 640 °C.

Luminescent Properties

Metal–organic polymeric complexes with d^{10} ions [Zn^{II}, Cd^{II}, Ag^I, and so on] have been found to be promising luminescent materials with potential application as, for example, light-emitting materials.[18] In the present work, the emission spectra of complexes **1**, **2**, **4**, **6**, **7**, and the free ligand **L** in the solid state at room temperature were investigated (Figure 6). All complexes were excited at ca. 287 nm, and the main emission bands of the complexes were located at ca. 394 nm. These emissions are neither metal-to-ligand charge transfer (MLCT) nor ligand-to-metal charge transfer (LMCT), but they may be assigned to intraligand (n–π* or π–π*) emission because similar emissions are observed at 396 nm for the free ligand **L** when excited at 290 nm.[19]

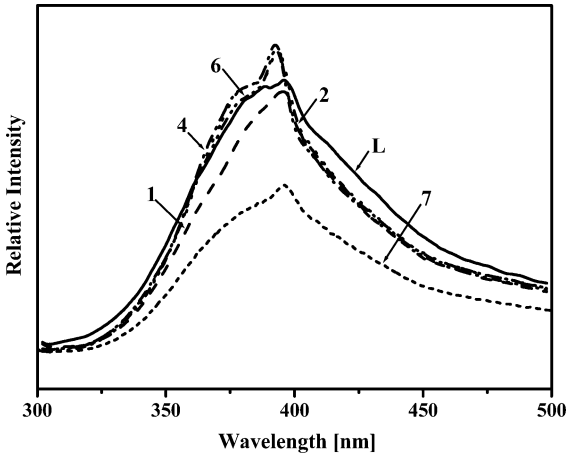

Figure 6. Emission spectra of complexes (**1**, **2**, **4**, **6**, and **7**) and ligand L in the solid state at room temperature.

EPR Spectroscopy

It is well known that transition-metal complexes are often paramagnetic, as they have partly occupied d orbitals; thus, they possess unpaired electron spins. The paramagnetism of such species makes them amenable to electron paramagnetic resonance (EPR) spectroscopy, which is one of the most successful tools used to investigate magnetic properties.[20] The X-band EPR spectrum of the powdered sample of complex **5** was studied at room temperature. The crystal structure of complex **5** shows that the Mn^{II} ion is isolated (although **5** is a 2D coordination polymer, because the bridges are very long; thus, the *J* parameter will be zero or negligible). The Mn^{II} ion has $S = 5/2$. By applying the ZFS, a qualitative scheme can be found (Supporting Information, Figure S12). It could be seen that there are two possible signals that can become one if the separation between –3/2 and –1/2 is something different. This scheme is only for B (H) (magnetic field) applied parallel to *z*. Thus, there is another scheme for a magnetic field applied perpendicular to *z*. In this case, however, the curves are very difficult to draw. As a consequence, with an *h* value that is more or less half the value of *D*, two of four signals must be found. The simulation gives the following parameters: $|D| = 0.30$ cm^{-1}, $g(\perp) = 2.25$, $g(\|) = 2.08$, and bandwidth = 800 Gauss (Figure 7). All parameters are consistent with the reported values that

have a slightly distorted octahedral environment with the unpaired electron occupying d orbitals in the solid state.[20b] Some small bands are not possible to simulate, because they can only be approximated, and the system is not completely isolated.

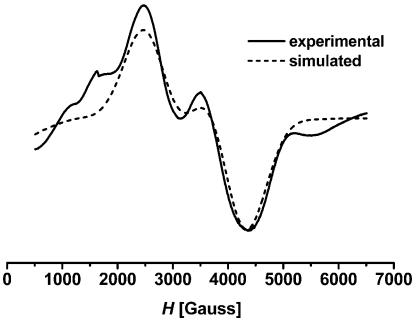

Figure 7. EPR spectra of complex **5** at room temperature.

Conclusions

Seven complexes with the flexible ligand 2,3-bis(triazol-1-ylmethyl)quinoxaline (**L**) were reported. The results show that the metal ions and counteranions have an important influence on the structures of the complexes; therefore, they must be taken into account when designing new metal–organic architectures. Moreover, complexes **1**, **2**, **4**, **6**, **7**, as well as the free ligand **L** display fluorescent emission in the solid state at room temperature.

Experimental Section

Materials and Physical Measurements: All reagents and solvents employed were commercially available and used as received without further purification. Elemental analyses of C, H, and N were performed with a Perkin–Elmer 240C analyzer. IR spectra were measured with a TENSOR 27 (Bruker) FTIR spectrometer with KBr pellets in the range 4000–400 cm^{-1}. ^1H NMR spectra were recorded with a Bruker AC-P 300 spectrometer (300 MHz) in $CDCl_3$ medium at 25 °C with tetramethylsilane as the internal reference. The X-ray powder diffraction (XRPD) was recorded with a Rigaku D/Max-2500 diffractometer at 40 kV, 100 mA for a Cu-target tube and a graphite monochromator. Simulation of the XRPD spectra was carried out by the single-crystal data and mercury (1.4.2) program. Thermal stability (TG-DTA) studies were carried out with a Dupont thermal analyzer from room temperature to 800 °C. Solid-state fluorescence spectra were recorded with a Cary Eclipse spectrofluorometer (Varian) equipped with a xenon lamp and a quartz carrier at room temperature. Electron paramagnetic resonance (EPR) measurements at X-band frequency were obtained with a Bruker EMX 6/1 spectrometer.

2,3-Bis(triazol-1-ylmethyl)quinoxaline (L): Triazole (50 mmol), aqueous potassium hydroxide (25%, 7.5 mL), and 2,3-bis(bromomethyl)quinoxaline (10 mmol) were added to acetonitrile (80 mL), and the mixture was then stirred at room temperature for 3 d. After completion of the reaction, the mixture was evaporated in vacuo, and the crude product was purified by recrystallization from chloroform/hexane. Yield: 1.84 g (63%). M.p. 152–153 °C. ^1H NMR (300 MHz, $CDCl_3$): δ = 5.93 (s, 4 H), 7.79–7.83 (m, 2 H), 7.98 (s, 2 H), 8.04–8.07 (m, 2 H), 8.39 (s, 2 H) ppm. IR (KBr): $\tilde{\nu}$ = 3078 (m), 1508 (s), 1444 (s), 1338 (w), 1277 (s), 1207 (m), 1135 (s), 958 (w), 897 (m), 855 (m), 777 (s), 710 (m), 679 (s), 643 (w) cm^{-1}. $C_{14}H_{12}N_8$ (292.3): calcd. C 57.53, H 4.14, N 38.34; found C 57.67, H 3.98, N 38.55.

Preparation of Complexes 1–7

$[ZnLCl_2]_2$ (1): A buffer layer of a solution of methanol and chloroform (1:1, 5 mL) was carefully layered over a chloroform (5 mL) solution of **L** ligand (0.1 mmol). Then, a solution of $ZnCl_2$ (0.1 mmol) in methanol (5 mL) was layered over the buffer layer. The solution was left for about two weeks at room temperature, and yellow block crystals were obtained. Yield: 13 mg (≈30%, based on **L**). IR (KBr): $\tilde{\nu}$ = 3438 (br.), 3162 (w), 3124 (m), 1531 (m), 1438 (s), 1287 (m), 1214 (w), 1131 (s), 999 (s), 882 (m), 849 (m), 780 (s), 720 (w), 673 (m), 633 (w), 438 (w) cm^{-1}. $C_{28}H_{24}N_{16}Cl_4Zn_2$ (857.17): calcd. C 39.23, H 2.82, N 26.14; found C 39.57, H 2.58, N 25.88.

$\{[M(L)_2(NO_3)_2]\}_\infty$ [M = Zn (2), Mn (3)]: A solution of $M(NO_3)_2$ [$Zn(NO_3)_2{\cdot}6H_2O$ for **2**, $Mn(NO_3)_2{\cdot}6H_2O$ for **3**] (0.1 mmol) in methanol (10 mL) was added to a solution of **L** (0.1 mmol) in chloroform (10 mL) at room temperature. The mixture was stirred for about 30 min and then filtered. The clear filtrate was allowed to stand for about two weeks at room temperature, from which colorless block crystals suitable for X-ray analysis were obtained. For **2**: Yield: 12 mg (≈30%, based on **L**). IR (KBr): $\tilde{\nu}$ = 3445 (br.), 3139 (m), 2995 (w), 1531 (m), 1435 (s), 1370 (s), 1274 (m), 1213 (w), 1129 (s), 1044 (m), 1017 (m), 991 (m), 879 (s), 856 (m), 808 (w), 778 (m), 704 (m), 676 (s), 647 (w), 426 (w) cm^{-1}. $C_{28}H_{24}N_{18}O_6Zn$ (774.02): calcd. C 43.45, H 3.13, N 32.57; found C 43.13, H 3.44, N 32.82. For **3**: Yield: 10 mg (≈20%, based on **L**). IR (KBr): $\tilde{\nu}$ = 3437 (br.), 3143 (m), 2999 (m), 1529 (m), 1439 (s), 1375 (s), 1281 (m), 1222 (m), 1137 (s), 1109 (s), 987 (w), 881 (m), 857 (w), 808 (w), 768 (s), 677 (m), 624 (m), 426 (w) cm^{-1}. $C_{28}H_{24}N_{18}O_6Mn$ (763.59): calcd. C 44.05, H 3.17, N 33.02; found C 44.41, H 3.35, N 32.77.

$\{[M(L)_2(H_2O)_2](ClO_4)_2(CH_3COCH_3)_2\}_\infty$ [M = Zn (4), Mn (5)] and $\{[Cd(L)_2(H_2O)_2](ClO_4)_2(H_2O)_6\}_\infty$ (6): Colorless block crystals suitable for X-ray analysis were obtained by using a similar method to that described for **1**, except acetone was used instead of methanol as the solvent, and $M(ClO_4)_2{\cdot}6H_2O$ [M = Zn (**4**), Cd (**5**), Mn (**6**)] instead of $ZnCl_2$. For **4**: Yield: 15 mg (≈30%, based on **L**). IR (KBr): $\tilde{\nu}$ = 3444 (br.), 3148 (m), 1699 (m), 1638 (m), 1532 (m), 1437 (s), 1290 (m), 1223 (w), 1137 (s), 1105 (s), 882 (m), 857 (w), 769 (m), 705 (w), 677 (m), 624 (s) cm^{-1}. $C_{34}H_{40}Cl_2N_{16}O_{12}Zn$ (1001.09): calcd. C 40.79, H 4.03, N 22.39; found C 40.96, H 3.86, N 22.14. For **5**: Yield: 15 mg (≈30%, based on **L**). IR (KBr): $\tilde{\nu}$ = 3444 (br.), 3143 (m), 1699 (m), 1641 (w), 1529 (m), 1438 (s), 1281 (m), 1222 (m), 1138 (s), 1108 (s), 987 (w), 881 (m), 857 (w), 768 (m), 704 (w), 676 (m), 624 (m) cm^{-1}. $C_{34}H_{40}Cl_2N_{16}O_{12}Mn$ (990.67): calcd. C 41.22, H 4.07, N 22.62; found C 40.94, H 4.32, N 22.45. For **6**: Yield: 16 mg (≈30%, based on **L**). IR (KBr): $\tilde{\nu}$ = 3445 (br.), 3142 (m), 1699 (w), 1647 (w), 1530 (m), 1439 (s), 1282 (w), 1218 (w), 1137 (s), 1107 (s), 987 (w), 881 (m), 858 (w), 768 (m), 705 (w), 674 (m), 624 (m) cm^{-1}. $C_{28}H_{40}Cl_2N_{16}O_{16}Cd$ (1040.69): calcd. C 32.34, H 3.88, N 21.55; found C 32.57, H 3.61, N 21.36.

$\{[AgL]\ (ClO_4)\ (H_2O)_{1.5}\}_\infty$ (7): Colorless block crystals suitable for X-ray analysis were obtained by using the similar method to that described for **1**, except $Ag(ClO_4){\cdot}H_2O$ was used instead of $ZnCl_2$, and the reaction was kept in darkness. Yield: 17 mg (≈30%, based on **L**). IR (KBr): $\tilde{\nu}$ = 3454 (br.), 1634 (m), 1513 (s), 1436 (s), 1313 (w), 1276 (s), 1212 (s), 1140 (s), 1090 (s), 1017 (m), 968 (w), 856 (m),

Table 2. Crystal data and structure refinement parameters for complexes **1**–**7**.

	1	**2**	**3**	**4**
Formula	$C_{28}H_{24}Zn_2N_{16}Cl_4$	$C_{28}H_{24}ZnN_{18}O_6$	$C_{28}H_{24}MnN_{18}O_6$	$C_{34}H_{40}ZnN_{16}Cl_2O_{12}$
Fw	857.17	774.02	763.59	1001.09
Crystal system	triclinic	monoclinic	monoclinic	monoclinic
Space group	$P\bar{1}$	$P2/n$	$P2/n$	$C2/c$
a [Å]	6.8312(14)	14.224(3)	14.215(3)	32.855(5)
b [Å]	8.8918(18)	7.3856(14)	7.3867(15)	8.3309(14)
c [Å]	13.958(3)	16.853(3)	16.862(3)	18.313(3)
α [°]	100.73(3)	90	90	90
β [°]	102.25(3)	113.880(3)	113.93(3)	118.628(3)
γ [°]	94.80(3)	90	90	90
V [Å^{-3}]	807.3(3)	1618.8(5)	1618.4(6)	4399.8(12)
Z	1	2	2	4
D [g cm^{-3}]	1.763	1.588	1.567	1.511
μ [mm^{-1}]	1.868	0.833	0.483	0.758
T [K]	293(2)	293(2)	293(2)	293(2)
R[a]/wR[b]	0.0315/0.0785	0.0352/0.0783	0.0602/0.1540	0.0516/0.1247
Total/unique/R_{int}	6241/3781/0.0262	8051/2851/0.0424	9412/2792/0.0551	10814/3860/0.0463
F(000)	432	792	782	2064
	5	**6**	**7**	
Formula	$C_{34}H_{40}MnN_{16}Cl_2O_{12}$	$C_{28}H_{40}CdN_{16}Cl_2O_{16}$	$C_{28}H_{30}Ag_2Cl_2N_8O_{11}$	
Fw	990.67	1040.09	1047.27	
Crystal system	monoclinic	monoclinic	monoclinic	
Space group	$C2/c$	$C2/c$	$C2/c$	
a [Å]	33.190(7)	33.199(7)	21.231(15)	
b [Å]	8.3257(17)	8.4704(17)	13.901(9)	
c [Å]	18.598(4)	18.515(4)	14.122(10)	
α [°]	90	90	90	
β [°]	118.913(3)	118.096(3)	105.511(13)	
γ [°]	90	90	90	
V [Å^3]	4499.1(16)	4593.2(16)	4016(5)	
Z	4	4	4	
D [g cm^{-3}]	1.457	1.481	1.732	
μ [mm^{-1}]	0.488	0.671	1.184	
T [K]	293(2)	293(2)	293(2)	
R[a]/wR[b]	0.0773/0.1977	0.0545/0.1525	0.0847/0.2126	
Total/unique/R_{int}	16280/3942/0.0507	11309/4032/0.015	9402/3474/0.1372	
F(000)	432	2056	2080	

[a] $R = \Sigma(||F_o| - |F_C||)/\Sigma|F_o|$. [b] $wR = [\Sigma w(|F_o|^2 - |F_C|^2)^2/\Sigma w(F_o^2)]^{1/2}$.

778 (s), 679 (s), 627 (s) cm^{-1}. $C_{14}H_{15}ClN_8O_{5.5}Ag$ (526.64): calcd. C 31.93, H 2.87, N 21.28; found C 31.74, H 3.14, N 20.85.

Caution! Perchlorate complexes of metal ions in the presence of organic ligands are potentially explosive. Only a small amount of material should be used and handled with care.

X-ray Crystallography: X-ray single-crystal diffraction data for **1**–**7** were collected with a Bruker Smart 1000 CCD diffractometer at room temperature with Mo-K_α radiation (λ = 0.71073 Å) by ω scan mode. The program SAINT[21] was used for integration of the diffraction profiles. Semi-empirical absorption corrections were applied by using the SADABS program. All structures were solved by direct methods with the use of the SHELXS program of the SHELXTL package and refined by full-matrix least-squares methods with SHELXL.[22] Metal atoms in each complex were located from the *E*-maps and other non-hydrogen atoms were located in successive difference Fourier syntheses and refined with anisotropic thermal parameters on F^2. Hydrogen atoms of carbon were included in calculated positions and refined with fixed thermal parameters riding on their parent atoms. The hydrogen atoms of part of solvent were located from Fourier difference maps with suitable restraint, and part of those could not be located in the difference map. Crystallographic data and experimental details for structural analyses are summarized in Table 2. Selected bond lengths and angles for **1**–**7** are listed in Table 1. CCDC-644956, 644957, 644958, 644959, 644960, -644961, and -658027 contain the supplementary crystallographic data for this paper. These data can be obtained free of charge from The Cambridge Crystallographic Data Centre via www.ccdc.cam.ac.uk/data_request/cif.

Supporting Information (see also the footnote on the first page of this article): XRPD patterns of **1**, **2**, **4**, **5**, **6**, and **7**, TG-DTA curves of **1**, **2**, **4**, **6**, and **7**, and qualitative scheme for **5**.

Acknowledgments

This work is supported by NSFC (No. 50673043 and No. 20531040), the Natural Science Fund of Tianjin, China (Key project, no. 07JCZDJC00500). We greatly thank Prof. Joan Ribas for his kind help in simulating and explaining the EPR spectrum.

[1] For examples, see: a) L. Pan, B. Parker, X. Y. Huang, D. H. Olson, J. Y. Lee, J. Li, *J. Am. Chem. Soc.* **2006**, *128*, 4180–4181; b) T. Wu, B. H. Yi, D. Li, *Inorg. Chem.* **2005**, *44*, 4130–4132; c) M. Fujita, T. M. Ominaga, K. Suzuki, M. Kawano, T. Kusukawa, *Angew. Chem. Int. Ed.* **2004**, *43*, 5621–5625; d) X. L. Wang, C. Qin, N. B. Wang, *Angew. Chem. Int. Ed.* **2005**, *44*, 5824–5827; e) X.-H. Bu, M.-L. Tong, H.-C. Chang, S. Kita-

gawa, S. R. Batten, *Angew. Chem. Int. Ed.* **2004**, *43*, 192–195; f) S. Das, P. K. Bharadwaj, *Inorg. Chem.* **2006**, *45*, 5257–5259.
[2] For examples, see: a) N. W. Ockwig, O. Delgado-Friederichs, M. O'Keeffe, O. M. Yaghi, *Acc. Chem. Res.* **2005**, *38*, 176–182; b) O. R. Evans, W. B. Lin, *Acc. Chem. Res.* **2002**, *35*, 511–522; c) K. Kasai, M. Aoyagi, M. Fujita, *J. Am. Chem. Soc.* **2000**, *122*, 2140–2147; d) S. Kitagawa, R. Kitaura, S. I. Noro, *Angew. Chem. Int. Ed.* **2004**, *43*, 2334–2375; e) Q. Ye, X. S. Wang, H. Zhao, R. G. Xiong, *Chem. Soc. Rev.* **2005**, *34*, 208–225.
[3] For examples, see: a) J. J. Wolff, *Angew. Chem. Int. Ed. Engl.* **1996**, *35*, 2195–2197; b) M. E. Davis, *Chem. Eur. J.* **1997**, *3*, 1745–1750; c) D. L. Caulder, K. N. Raymond, *Acc. Chem. Res.* **1999**, *32*, 975–982; d) N. Lalioti, C. P. Raptopoulou, A. Terzis, A. E. Aliev, I. Gerothanassis, P. E. Manessi-Zoupa, S. P. Perlepes, *Angew. Chem. Int. Ed.* **2001**, *40*, 3211–3214; e) W. T. Chen, G. C. Guo, M. S. Wang, G. Xu, L. Z. Cai, T. Akitsu, M. Akita-Tanaka, A. Matsushita, J. S. Huang, *Inorg. Chem.* **2007**, *46*, 2105–2114.
[4] a) J. F. Ma, J. F. Liu, X. Yan, H. Q. Jia, Y. H. Lin, *J. Chem. Soc. Dalton Trans.* **2000**, 2403–2407; b) M. C. Hong, Y. J. Shako, W. P. Su, R. Cao, M. Fujita, Z. Y. Zhou, A. S. C. Chan, *Angew. Chem. Int. Ed.* **2000**, *39*, 2468–2470.
[5] A. J. Blake, N. R. Champness, P. Hubberstey, W. S. Li, M. A. Withersby, M. Schröder, *Coord. Chem. Rev.* **1999**, *183*, 117–138.
[6] a) K. A. Hirsch, S. R. Wilson, J. S. Moore, *Chem. Eur. J.* **1997**, *3*, 765–771; b) L. Carlucci, G. Ciani, P. Macchi, D. M. Proserpio, S. Rizzato, *Chem. Eur. J.* **1999**, *5*, 237–243; c) M. A. Withersby, A. J. Blake, N. R. Champness, P. Hubberstey, W. S. Li, M. Schröder, *Angew. Chem. Int. Ed. Engl.* **1997**, *36*, 2327–2329; d) Y.-N. Chi, K.-L. Huang, F.-Y. Cui, Y.-Q. Xu, C.-W. Hu, *Inorg. Chem.* **2006**, *45*, 10605–10612.
[7] a) J. Lu, T. Paliwala, S. C. Lim, C. Yu, T. Niu, A. J. Jacobson, *Inorg. Chem.* **1997**, *36*, 923–929; b) O. S. Jung, S. H. Park, K. M. Kim, H. G. Jang, *Inorg. Chem.* **1998**, *37*, 5781–5785; c) T. L. Hennigar, D. C. MacQuarrie, P. Losier, R. D. Roger, M. J. Zaworkto, *Angew. Chem. Int. Ed. Engl.* **1997**, *36*, 972–973.
[8] a) R. W. Saalfrank, I. Bernt, M. M. Chowdhury, F. Hammpel, G. B. M. Vaughan, *Chem. Eur. J.* **2001**, *7*, 2765–2769; b) A. J. Black, N. R. Brooks, N. R. Champness, P. A. Cooke, A. M. Deveson, D. Fenske, P. Hubberstey, W. S. Li, M. Schröder, *J. Chem. Soc. Dalton Trans.* **1999**, 2103–2110.
[9] a) N. Matsumoto, Y. Motoda, T. Matsuo, T. Nakashima, N. Re, F. Dahan, J. P. Tuchagues, *Inorg. Chem.* **1999**, *38*, 1165–1173; b) L. Pan, X. Y. Huang, J. Li, Y. G. Wu, N. W. Zheng, *Angew. Chem. Int. Ed.* **2000**, *39*, 527–530; c) S. J. Dalgarno, M. J. Hardie, C. L. Raston, *Cryst. Growth Des.* **2004**, *4*, 227–234.
[10] a) Y. B. Dong, Y. Y. Jiang, J. P. Ma, F. L. Liu, B. Tang, R. Q. Huang, S. R. Batten, *J. Am. Chem. Soc.* **2007**, *129*, 4520–4521; b) M. L. Tong, S. Hu, J. Wang, S. Kitagawa, S. W. Ng, *Cryst. Growth Des.* **2005**, *5*, 837–839.
[11] a) P. Díaz, J. Benet-Buchholz, R. Vilar, A. J. P. White, *Inorg. Chem.* **2006**, *45*, 1617–1626; b) H. J. Kim, W. C. Zin, M. Lee, *J. Am. Chem. Soc.* **2004**, *126*, 7009–7014; c) S. J. Coles, J. G. Frey, P. A. Gale, M. B. Hursthouse, M. E. Light, K. Navakhun, G. L. Thomas, *Chem. Commun.* **2003**, 568–569; d) P. A. Gale, *Coord. Chem. Rev.* **2003**, *240*, 191–221; e) R. Vilar, *Angew. Chem. Int. Ed.* **2003**, *42*, 1460–1477; f) J. L. Atwood, A. Szumna, *Chem. Commun.* **2003**, 940–941; g) M. Schweiger, S. R. Seidel, A. M. Arif, P. J. Stang, *Inorg. Chem.* **2002**, *41*, 2556–2559.
[12] For examples, see: a) L. Han, M. C. Hong, *Inorg. Chem. Commun.* **2005**, *8*, 406–419; b) B. Moulton, M. J. Zaworotko, *Chem. Rev.* **2001**, *101*, 1629–1658; c) H. W. Hou, Y. L. Wei, Y. L. Song, Y. T. Fan, Y. Zhu, *Inorg. Chem.* **2004**, *43*, 1323–1327; d) C. W. Lim, S. Sakamoto, K. Yamaguchi, J. I. Hong, *Org. Lett.* **2004**, *6*, 1079–1082; e) J. Hausmann, G. B. Jameson, S. Brooker, *Chem. Commun.* **2003**, 2992–2993; f) C. Y. Su, M. D. Smith, H. C. zur Loye, *Angew. Chem. Int. Ed.* **2003**, *42*, 4085–4089; g) M. X. Li, P. Cai, C. Y. Duan, F. Lu, J. Xie, Q. J. Meng, *Inorg. Chem.* **2004**, *43*, 5174–5176; h) A. V. Davis, K. N. Raymond, *J. Am. Chem. Soc.* **2005**, *127*, 7912–7919.
[13] For examples, see: a) K. M. Fromm, J. L. Sagué Doimeadios, A. Y. Robin, *Chem. Commun.* **2005**, 4548–4550; b) B. C. Zeng, B. S. Chen, S. Y. Lee, W. H. Liu, G. H. Lee, S. M. Peng, *New J. Chem.* **2005**, *29*, 1254–1257; c) L. Hou, D. Li, *Inorg. Chem. Commun.* **2005**, *8*, 190–193; d) Q. G. Zhai, C.-Z. Lu, S.-M. Chen, X.-J. Yang, W.-B. Xu, *Cryst. Growth Des.* **2006**, *6*, 1393–1398.
[14] For examples, see: a) C. Y. Su, Y. P. Cai, C. L. Chen, M. D. Smith, W. Kaim, H. C. zur Loye, *J. Am. Chem. Soc.* **2003**, *125*, 8595–8613; b) Z. H. Zhang, Y. Song, T. Okamura, Y. Hasegawa, W. Y. Sun, N. Ueyama, *Inorg. Chem.* **2006**, *45*, 2896–2902; c) B. Z. Li, J. H. Zhou, B. L. Li, Y. Zhang, *J. Mol. Struct.* **2004**, *707*, 187–; d) B. L. Li, Y. F. Peng, B. Z. Li, Y. Zhang, *Chem. Commun.* **2005**, 2333–2335.
[15] a) X. R. Meng, Y. L. Song, H. W. Hou, H. Y. Han, B. Xiao, Y. T. Fan, Y. Zhu, *Inorg. Chem.* **2004**, *43*, 3528–3536; b) B. F. Hoskins, R. Robson, D. A. Slizys, *J. Am. Chem. Soc.* **1997**, *119*, 2952–2953.
[16] a) D. Z. Wang, C. S. Liu, J. R. Li, L. Li, Y. F. Zeng, X. H. Bu, *CrystEngComm* **2007**, *9*, 289–297; b) C. Y. Li, C. S. Liu, J. R. Li, X. H. Bu, *Cryst. Growth Des.* **2007**, *7*, 286–295; c) T. L. Hu, J. R. Li, Y. B. Xie, X. H. Bu, *Cryst. Growth Des.* **2006**, *6*, 648–655; d) G. H. Cui, J. R. Li, J. L. Tian, X. H. Bu, S. R. Batten, *Cryst. Growth Des.* **2005**, *5*, 1775–1780; e) Y. Zheng, J. R. Li, M. Du, R. Q. Zou, X. H. Bu, *Cryst. Growth Des.* **2005**, *5*, 215–222.
[17] V. Balamurugan, M. S. Hundal, R. Mukherjee, *Chem. Eur. J.* **2004**, *10*, 1683–1690.
[18] For examples, see: a) M. Altmann, U. H. F. Bunz, *Angew. Chem. Int. Ed. Engl.* **1995**, *34*, 569–571; b) U. H. F. Bunz, *Chem. Rev.* **2000**, *100*, 1605–1644; c) R. L. Sang, L. Xu, *Inorg. Chem.* **2005**, *44*, 3731–3737; d) D. M. Ciurtin, N. G. Pschirer, M. D. Smith, U. H. F. Bunz, H. C. zur Loye, *Chem. Mater.* **2001**, *13*, 2743–2745; e) F. Würthner, A. Sautter, *Chem. Commun.* **2000**, 445–446.
[19] a) Y. B. Dong, H. Y. Wang, J. P. Ma, D. Z. Shen, R. Q. Huang, *Inorg. Chem.* **2005**, *44*, 4679–4692; b) C. D. Wu, H. L. Ngo, W. B. Lin, *Chem. Commun.* **2004**, 1588–1589.
[20] a) A. Abragam, B. Bleaney, *Electron Paramagnetic Resonance of Transition Ions*, Dover Publications, Inc., New York, **1986**; b) J. Krzystek, A. Ozarowski, J. Telser, *Coord. Chem. Rev.* **2006**, *250*, 2308–2324.
[21] Bruker AXS, *SAINT Software Reference Manual*, Madison, WI, **1998**.
[22] G. M. Sheldrick, *SHELXTL NT: Program for Solution and Refinement of Crystal Structures*, *Version 5.1*, University of Göttingen, Germany, **1997**.

Received: September 6, 2007
Published Online: January 7, 2008

